Metal Halide Perovskites for Solar-to-Chemical Fuel Conversion

*Jie Chen, Chunwei Dong, Hicham Idriss, Omar F. Mohammed, and Osman M. Bakr**

Dr. J. Chen, C. W. Dong, Prof. O. F. Mohammed, Prof. O. M. Bakr
King Abdullah University of Science and Technology (KAUST), Division of Physical Science and Engineering (PSE), Thuwal 23955-6900, Saudi Arabia.
E-mail: osman.bakr@kaust.edu.sa
Dr. J. Chen, C. W. Dong, Prof. O. M. Bakr
KAUST Catalysis Center, Thuwal 23955-6900, Saudi Arabia.
Prof. H. Idriss
Fundamental Catalysis, Centre for Research and Development (CRD), SABIC, Thuwal 23955-6900, Saudi Arabia.

Keywords: solar fuel conversion, halide perovskite, CO_2 reduction, proton reduction

Abstract: This article comprehensively summarizes the recent progress made in the stabilization, protection, improvement and design of halide perovskites-based photocatalysts, photoelectrodes and devices for solar-to-chemical fuel conversion. With the target at water splitting, HI splitting and CO_2 reduction reactions, the strategies established for halide perovskites used in photocatalytic particle-suspension systems, photoelectrode thin-film systems and photovoltaic-(photo)electrocatalysis tandem systems are systematically organized and introduced. Moreover, the recent achievements in discovering new and stable halide perovskite materials, developing protective and functional shells and layers, designing proper reaction solution systems and tandem device configurations are emphasized and discussed. The perspectives on the future design of halide perovskite materials and devices for solar-to-chemical fuel conversion are further provided. This review will serve as a guideline for researchers who are currently focusing on halide perovskite materials as well as for those who are interested in solar-to-chemical fuel conversion.

1. Introduction

Efficient conversion of solar energy to chemical fuels on a scale on par with the energy supplied from conventional fossil fuels is a promising yet challenging pathway to realizing a sustainable carbon-neutral society.[1-7] The main chemical energy carriers in this pathway are H_2 and various C_1-C_3 compounds, which have either high energy densities or versatile applications in industry but require thermodynamically uphill water splitting or CO_2 reduction reactions to be produced.[5-9] To date, several solar-chemical fuel conversion systems, including photocatalyst particle-suspension, photoelectrode thin-film and photovoltaic-electrocatalysis systems, have been developed to meet the requirements of certain reactions and have been optimized for practical use.[5, 8] Although the system configurations vary, the key element to a solar-chemical fuel conversion system is the semiconductor material, which converts solar energy to excited electrons and holes that then separate to drive uphill reduction and oxidation reactions.[2, 10, 11]

Metal halide perovskites with a general formula of ABX_3 (**Figure 1**a)—where A is methylammonium (MA), formamidinium (FA) or Cs; B is Pb or Sn; and X is Cl, Br or I—have recently emerged as a promising class of high-performance semiconductors since the first solar cell involving $MAPbI_3$ was reported.[12] These perovskites have remarkable photophysical, optical, and transport properties, such as long charge carrier lifetimes and low trap densities,[13, 14] long electron and hole diffusion lengths,[15-17] large absorption coefficients[18, 19] and a widely tunable bandgap that enables light harvesting from UV all the way to near IR spectral range[20, 21] (Figure 1b). More importantly, the band positions of most halide perovskites satisfy the thermodynamic requirements for water and CO_2 reduction, as shown in Figure 1c.

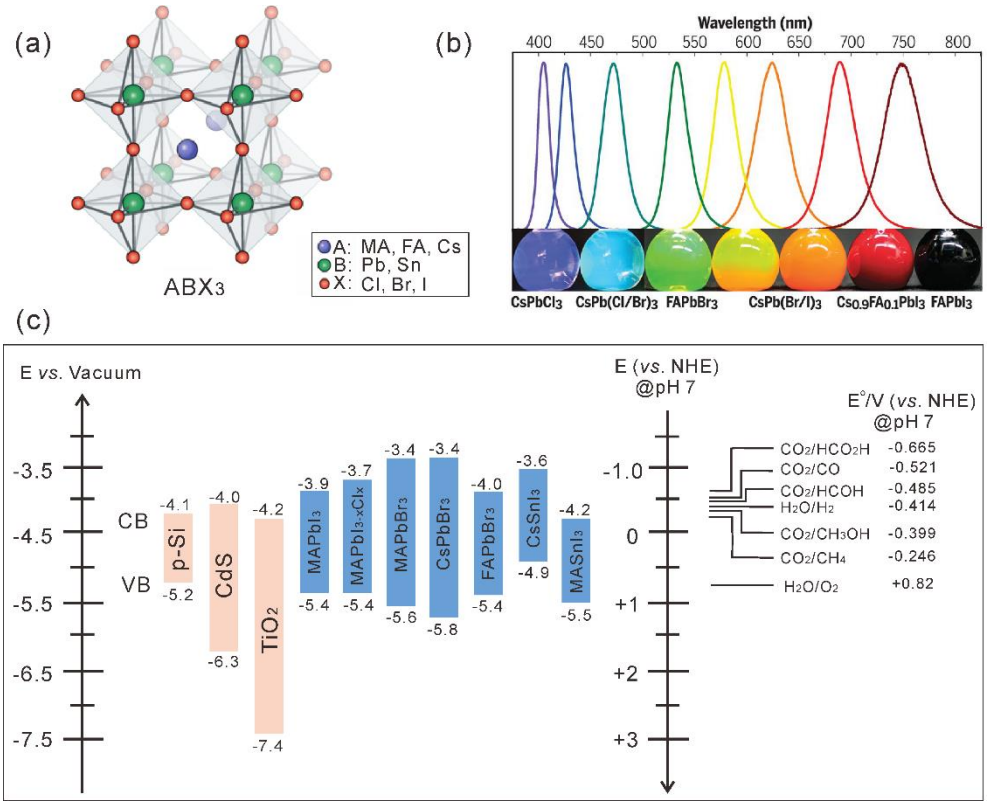

Figure 1. (a) The general crystal structure of the 3D halide perovskite ABX_3. Reprinted with permission from Ref.[20] Copyright 2019, Nature Publishing Group. (b) Photoluminescence spectra and corresponding photographs of composition-tuned halide perovskite nanocrystals. Reprinted with permission from Ref.[21] Copyright 2017, AAAS. (c) Conduction band (CB) and valence band (VB) potentials of representative semiconductors and halide perovskites for solar-chemical fuel conversion (p-Si, CdS, TiO_2). The relative potentials of the CO_2 and water redox couples at pH 7 are plotted vs. vacuum (left) and normal hydrogen electrode (NHE) (right).

By virtue of their impressive photophysical properties, halide perovskites have been successfully used in various optoelectronic devices, including solution-processed solar cells with a power conversion efficiency (PCE) exceeding 24%,[22-25] low-threshold lasers,[26, 27] bright light-emitting diodes[28-30] and sensitive photo- and X-ray detectors.[31-34] This great success has also motivated the development of solar-chemical fuel conversion systems based on halide perovskites. However, the instability of halide perovskites upon exposure to water

and other polar solvents, irradiation, and heat has limited their study and applications in this sphere. To date, substantive efforts have been made to enable halide perovskites for solar-chemical fuel conversion. For example, halide perovskites powder suspensions were used in non-aqueous solutions for CO_2 reduction.[35] Moreover, halide perovskite photoelectrodes were protected by conductive layers for H_2O reduction[36] and CO_2 reduction.[37] In another instance, perovskite photovoltaics were used to drive electrocatalytic water splitting or CO_2 reduction by connecting an isolated photovoltaic cell to an electrocatalysis cell.[8] Despite this progress, the field is at its infancy and there is still much room for innovation in designing target reaction systems as well as in enhancing the stability and efficiency of halide perovskites for solar-to-chemical fuel conversion.

In this review, we summarize the advancements made to date in the development of halide perovskites for solar-chemical fuel conversion. The reactions involved in this process are water splitting, hydrogen iodide splitting, and CO_2 reduction. We classify and introduce the achievements made in incorporating halide perovskites into photocatalyst particle-suspension systems, photoelectrode thin-film systems and photovoltaic-(photo)electrocatalytic systems. We also introduce and discuss the syntheses and modification strategies established for yielding stable and efficient halide perovskites as well as the design of reaction system configurations. We hope that this work will inspire researchers to translate the benefits afforded by the remarkable photophysical properties of halide perovskites into highly efficient, selective, and stable solar-driven chemical fuel production.

2. Photocatalytic Particle-Suspension Systems

In 1979, Allen J. Bard designed the first photocatalyst particle-suspension system for water splitting[38] after Honda *et al.* had discovered what came to be known as the Honda-Fujishima effect in the early 1970s.[39] A photocatalytic reaction is carried out in a closed gas-circulation cell containing water as the proton or oxygen source, sacrificial reagents (if necessary) for half

oxidation or reduction reactions, semiconductor particles as the photocatalysts, and dissolved CO_2 (if the system is meant for CO_2 reduction).

Upon light irradiation, a semiconductor photocatalyst generates charge carriers (electrons and holes), see process (1) in **Figure 2**. Here, the energy of the incident light must exceed the bandgap energy of the semiconductor to allow for effective excitation. As the ΔG^0 values for water splitting and CO_2 reduction are 237 kJ/mol and 259 kJ/mol (taking the conversion of CO_2 to CO as an example), respectively, a theoretical band gap of at least 1.34 eV (corresponds to 954 nm) is required. Photoexcited charge carriers then migrate to the reactive sites for certain reactions, as shown in process (2) of Figure 2. Concomitant recombination [including bulk and surface recombination, process (2')] of the charge carriers (electron and hole) will also occur radiatively and/or non-radiatively, releasing photons or thermal energy. The electrons and holes reaching the reactive sites then undergo an electrochemical catalytic process to produce chemical fuels. Thermodynamically, such a process requires the electron potential (CB potential of the semiconductor) to be more negative than 0 V vs. NHE for reducing H^+ to H_2 (-0.107 V vs. NHE for CO_2 to CO, pH = 0), and the hole potential (VB potential) must be more positive than the oxidation potential of H_2O/O_2 (1.23 V vs. NHE, pH = 0). Generally, halide perovskites thermodynamically favor both the reduction and oxidation reactions, as their CB and VB straddle the water/CO_2 reduction and water oxidation potentials (Figure 1c). However, the complexity of the overall catalytic cycle requires the use of multiple components for kinetic reasons in addition to the above basic thermodynamic requirement in a real-experimental scenario. In this case, electrocatalysts (EC) such as Pt, MoS_2 and RuO_2 *et al.* are usually needed not only to extract electrons/holes from the semiconductors, but also to promote the kinetics for the catalytic reactions.

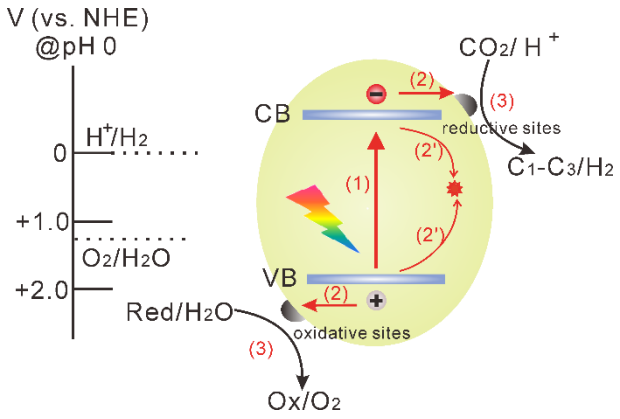

Figure 2. An illustration of charge transfer reactions that may occur at the surface and in the bulk of a metal/semiconductor photocatalyst. Why did you decide here to give the scale at pH 0 (while in figure 1 it is at pH 7)? Define the reductive and oxidation cycles. Can you give different numbers for 3 (may be 3 and 3') for consistency with 2 and 2'.

For photocatalyst particle-suspension systems, water/moisture instability issues associated with halide perovskites must be considered. Halide perovskites generally cannot resist water, even though some strategies can render them stable against a certain percentage of humidity.[40, 41] In this regard, researchers have expended great efforts by developing water-stable perovskite structures, discovering proper proton sources other than water and dispersing halide perovskite in non-aqueous solutions for CO_2 reduction.

2.1. Water-stable halide perovskites and their structures

Most of the reported halide perovskites have been recognized to dissolve like a salt in water. Encouragingly, Ju et al. have reported that $DMASnI_3$ ($DMA = CH_3NH_2CH_3^+$) can be suspended in deionized (DI) water for photocatalytic water splitting H_2 production with a rate of 0.64 μmol/h (200 mg catalysts) for at least 5 hours (**Figure 3**a).[42] The work also implied that $DMASnI_3$ can be a promising candidate for overall pure water splitting, as it was claimed in the article that SnI_4 is formed due to the formation of O_2 during the water splitting reactions. This is the first and only work in which a halide perovskite has been reported to be sufficiently stable

for water splitting, although the precise mechanism underlying this water stability is not yet clear. $ADPb_2Cl_5$ (AD = acridine), with a band gap of 2.06 eV, was also reported to be water-stable; however, the material was not used for solution-phase photocatalytic reactions.[43] $ADPb_2Cl_5$ is stable because the large steric hindrance exhibited by AD cations distributed between the rigid lead chloride inorganic matrices could effectively prevent erosion by water.

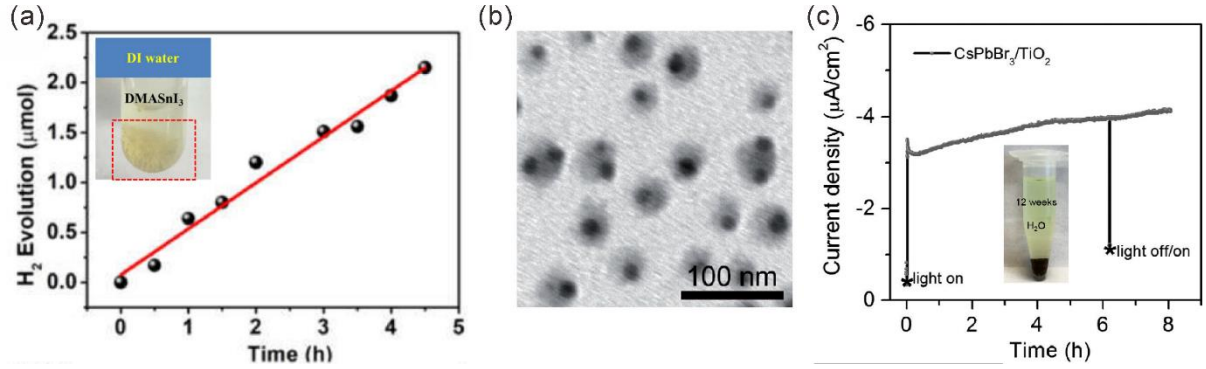

Figure 3. (a) Hydrogen production over $DMASnI_3$ crystals in DI water. Inset shows $DMASnI_3$ crystals dispersed in DI water. Reprinted with permission from Ref.[42] Copyright 2018, Wiley. (b) A TEM image of $CsPbBr_3@TiO_2$ core-shell nanocrystals (NCs) (I guess the grey structures are those of TiO2). (c) Controlled potential electrolysis of $CsPbBr_3@TiO_2$ NC electrode in neutral water over 8 h (why not simply chronoamperometry)). Inset shows a photograph of $CsPbBr_3@TiO_2$ in water for 12 weeks (what is the meaning or need of 12 weeks?). Figures (b) and (c) are reprinted with permission from Ref.[44] Copyright 2018, Wiley.

Strategies for protecting and functionalizing halide perovskites for photocatalysis have also been developed. One instant idea is to coat perovskite nanocrystals with a shell that is water-resistant, stable and photocatalytically active. Li et al. have coated colloidal $CsPbBr_3$ with a TiO_2 shell by hydrolysis and calcination of a titanium precursor (Figure 3b).[44] The $CsPbBr_3@TiO_2$ NCs were very stable and exhibited excellent water stability for more than 12 weeks, with size, morphology and crystallinity unchanged. More interestingly, the $CsPbBr_3@TiO_2$ NCs maintained a relatively constant photocurrent over 8 h under real-world

photoelectric test conditions in water (Figure 3c). Using a zeolitic imidazolate framework (ZIF) as the shell, Kong et al. have fabricated $CsPbBr_3$@ZIF core-shell structures by the in-situ growth of ZIF on $CsPbBr_3$ quantum dots (QDs).[45] The $CsPbBr_3$@ZIF composites were active and stable for the photocatalytic CO_2 reduction in the presence of CO_2 and H_2O vapor and exhibited electron consumption rates of 15.5 and 29.6 μmol/g/h for $CsPbBr_3$@ZIF-8 and $CsPbBr_3$@ZIF-67, respectively. Other perovskite@shell structures, such as $CsPbBr_3$@SiO_2[46] and $CsPbBr_3$@Al_2O_3[47, 48], have also been successfully synthesized; however, they have not been used as described above and might not be active for photocatalytic reactions because the SiO_2 or Al_2O_3 layers are not photocatalytic active.

2.2. Using proton sources other than water

Hydrogen iodide (HI) was first pointed out by Park *et al.* as a better choice than water for providing protons for H_2 production when employing $MAPbI_3$ as the photocatalyst.[49] $MAPbI_3$ is stable in a $MAPbI_3$-saturated aqueous HI solution because of the dynamic equilibrium between $MAPbI_3$ and HI. By dissolving a series of amounts of $MAPbI_3$ in HI, Park *et al.* obtained corresponding solubility data and proposed a dynamic equilibrium model for the $MAPbI_3$ to be stable in HI solution (**Figure 4**a-b). Moreover, the authors identified the conditions for the formation of stable $MAPbI_3$ precipitates in aqueous solution by controlling the I^- and H^+ concentrations ($[I^-] \leq [H^+]$, $pH \leq -0.5$, $-\log[I^-] \leq -0.4$). In aqueous HI solution, the $MAPbI_3$ powders could efficiently split HI into H_2 and I_3^- under visible-light irradiation according to a mechanism similar to water splitting (Figure 4c-d), and a solar HI splitting efficiency of 0.81% was achieved when using Pt as a cocatalyst.

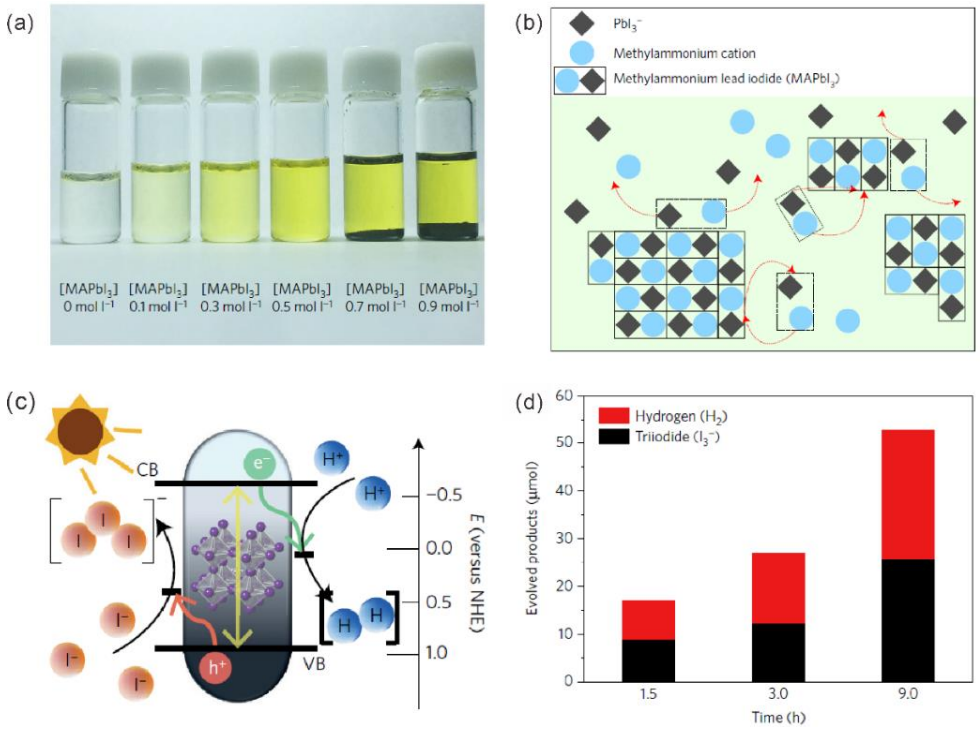

Figure 4. (a) $MAPbI_3$ in aqueous HI solution with different concentrations. (b) Schematic illustration of $MAPbI_3$ powder in dynamic equilibrium with a saturated HI solution. Dotted lines represent the dissolution and precipitation of $MAPbI_3$ crystals and ions. (c) Schematic band diagram of $MAPbI_3$ powder for the HI splitting photocatalytic reaction. (d) Quantitative comparison between the amounts of H_2 and I_3^- evolved at different reaction times. All figures are reprinted with permission from Ref.[49] Copyright 2016, Nature Publishing Group.

HI solution has been widely adopted by other researchers since the work of Park *et al*. For example, Huang *et al.* used HI and HBr/HI mixed solutions to test a modified $MAPbI_3$/rGO material[50] and the mixed halide perovskites $MAPbBr_{3-x}I_x$[51] and $CsPbBr_{3-x}I_x$.[52] Remarkably, $MAPbBr_{3-x}I_x$/Pt exhibited a photocatalytic H_2 evolution rate of 651.2 μmol/h (250 mg catalysts) under visible light (100 $mW \cdot cm^{-2}$, $\lambda \geq 420$ nm) and a solar-to-chemical conversion efficiency of 1.05%. Similarly, Wang et al. found that a high concentration of $MAPbBr_3$ can be stable in an aqueous solution of HBr, which can be split into H_2 and Br_2.[53] A high apparent quantum

efficiency of approximately 16.4% for H_2 evolution at 420 nm was achieved over their modified photocatalyst, Pt/Ta_2O_5-$MAPbBr_3$-PEDOT:PSS.

2.3. In non-aqueous reaction solutions

Non-aqueous solution systems with a trace amount of water (or in the complete absence of water) are usually designed for CO_2 reduction reactions. Ethyl acetate was selected by Su and co-workers for CO_2 reduction using $CsPbBr_3$ QDs/GO because of its mild polarity and high CO_2 solubility.[35] They reported that in ethyl acetate, $CsPbBr_3$ QDs catalyzed CO_2 reduction at an electron consumption rate of 23.7 μmol/g/h with a selectivity of over 99.3% for CO_2 reduction rather than for proton reduction. After compositing with GO, the rate of electron consumption increased by 25.5% because of the improved electron extraction and transport. Analogous solution systems have also been adapted to other types of halide perovskites, such as $Cs_2AgBiBr_6$[54] and $CsPbBr_3$.[35, 55] Ou et al. reported that acetonitrile with a trace amount of water (0.3 vol%) can also serve as a reaction solution for photocatalytic CO_2 reduction over halide perovskites.[56] The authors tested $CsPbBr_3$ QDs/g-C_3N_4 in acetonitrile/H_2O and achieved a 149 μmol/g/h CO production rate from CO_2 under visible-light irradiation. Wu et al. recently carried out the same reaction in ethyl acetate solution with a water content of 1.2 vol%.[57] At a saturated CO_2 in this medium, $MAPbI_3$@PCN-221(Fe_x) exhibited a total yield of 1559 μmol/g over an 80-h reaction period for CO (34%) and CH_4 (66%) production.

The photocatalytic water or HI splitting and CO_2 reduction performance of halide perovskites is summarized in **Table 1**. The as-developed halide perovskite photocatalysts generally exhibit enough stability to withstand a photocatalytic test. The photocatalysts' efficiencies are still quite low, especially considering the remarkable photophysical properties they possess. In addition, the conditions for the photocatalytic tests for different groups vary, thus making it difficult to fairly compare and evaluate the strategies researchers have applied

to improve the efficiency. Therefore, we strongly suggest that the community follow standard test conditions and/or provide detailed experimental procedures for photocatalytic reactions.

Table 1. Summary of the reported photocatalytic water or HI splitting and CO_2 reduction reactions using halide perovskites. Best to mention when O2 was measured in these experiments; or say that no O2 was quantitatively measured. This opens the question whether any of these studies are indeed catalytic. The field is driven by materials scientists most are not trained in catalysis and therefore neglect basic principles.

Materials	Reaction	Solution	Light source	Stability	Efficiency [a)]	Ref.
$DMASnI_3$	H_2O red. to H_2	DI water	300-W Xe lamp (full spectrum)	>5 h	3.2 μmol/g/h	[42]
$MAPbI_3$	HI red. to H_2	Aqueous HI (with Pt)	Solar simulator (≥ 475 nm)	160 h	57 μmol/g/h; Solar to chemical (0.81%)	[49]
$MAPbI_3$/rGO	HI red. to H_2	Aqueous HI	120 mW/cm^2 (≥ 420 nm)	200 h	939 μmol/g/h	[50]
$MAPbI_{3-x}Br_x$	HI red. to H_2	Aqueous HBr/HI (with Pt)	100 mW/cm^2 (≥ 420 nm)	> 30 h	2604 μmol/g/h; Solar to chemical (1.05%)	[51]
$CsPbI_{3-x}Br_x$	HBr red. to H_2	Aqueous HBr (with Pt)	120 mW/cm^2 (≥ 420 nm)	> 50 h	1120 μmol/g/h; AQE (2.5% @ 450 nm)	[52]

Pt/Ta_2O_5-$MAPbBr_3$-PEDOT: PSS	HBr red. to H_2	Aqueous HBr	150 mW/cm^2 (≥ 420 nm)	> 4 h	1050 μmol/g/h; AQE (16.4% @ 420 nm)	[53]
$CsPbBr_3$ QDs/GO	CO_2 red.	Ethyl acetate	150 mW/cm^2 (AM 1.5 G)	> 12 h	29.8 μmol/g/h	[35]
$Cs_2AgBiBr_6$ NCs	CO_2 red.	Ethyl acetate	150 mW/cm^2 (AM 1.5 G)	> 6 h	17.5 μmol/g/h	[54]
$CsPbBr_3$ QDs	CO_2 red.[b)]	Ethyl acetate, H_2O (0.3 vol%)	AM 1.5 G	> 8 h	20.9 μmol/g/h	[55]
$CsPbBr_3$ QDs/g-C_3N_4	CO_2 red.	Acetonitrile, H_2O (0.3 vol%)	300-W Xe lamp (≥ 420 nm)	> 6 h	149 μmol/g/h for CO production	[56]
$CsPbBr_3$@ZIF-67	CO_2 red.[b)]	H_2O, CO_2 vapor	150 mW/cm^2 (AM 1.5 G)	> 18 h	29.6 μmol/g/h	[45]
$CsPbBr_3$ QDs/UiO-66(NH_2)	CO_2 red.	Ethyl acetate, H_2O (0.3 vol%)	300-W Xe lamp (≥ 420 nm)	> 12 h	8.2 μmol/g/h for CO production	[58]
$MAPbI_3$@PCN-221(Fe_x)	CO_2 red.[c)]	Ethyl acetate, H_2O (1.2 vol%)	300-W Xe lamp (≥ 400 nm)	80 h	19.5 μmol/g/h	[57]

[a] For proton reduction, values pertain to the H_2 production rate; for CO_2 reduction, values pertain to the electron consumption rate unless otherwise noted. The rates were converted to μmol/g/h. [b] Oxygen was measured in these works but not quantified. [c] Oxygen generated was measured and quantified.

3. Photoelectrode Thin-Film Systems

The first demonstration of a photoelectrode thin-film system (also known as a photoelectrochemical cell) was by Fujishima and Honda in 1972 using a TiO_2 single-crystal wafer as the photoanode and Pt black as the cathode to split water under light irradiation and an applied bias.[39] A typical photoelectrochemical cell consists of a working electrode (i.e., photoelectrode), a counter electrode and a reference electrode (**Figure 5**). A photoelectrode can be fabricated by coating or growing several well-defined layers, such as a semiconductor layer, an electron/hole transport layer and an electrocatalytic layer, onto a conductive substrate. Figure 5 shows a cell structure in which the working electrode functions as a photocathode. In the cell, electrons from the photoexcited semiconductor are generated at the electrode for reduction reactions, whereas holes are at the counter electrode for oxidation reactions.

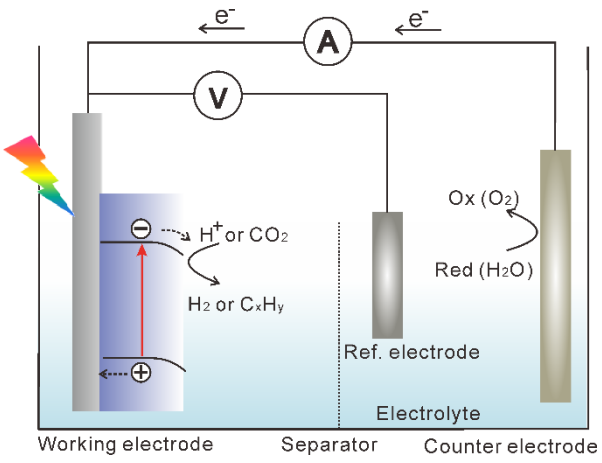

Figure 5. An illustration of a three-electrode photoelectrochemical (PEC) cell. The working electrode functions as a photocathode. What is a separator?

The photoelectrode structure greatly relieves the harsh stability requirements for halide perovskites used in aqueous solutions, as it is technically much easier to coat a water-impermeable, conductive and even catalytic layer onto the well-defined halide perovskite layer than onto the solution-phase nanocrystals. In practice, researchers indeed choose essentially the same strategy—coating layers onto a halide perovskite—to create stable halide perovskite photoelectrodes. To date, many types of such layers have been implemented, including a Ni layer (8 nm),[59] Field's metal (a fusible alloy that melts at approximately 62 °C.),[36] Ti foil,[60] an In-Bi alloy layer[37] and a mesoporous carbon/graphite sheet[61]. In the following, we discuss these approaches by classifying them according to their target reactions, i.e., water oxidation, water reduction or CO_2 reduction.

3.1.Water oxidation

Metal-based materials were first used to protect halide perovskite photoelectrodes. In 2015, Da et al. reported the first multilayered $MAPbI_3$-based photoanode with an ultrathin Ni surface layer deposited by magnetron sputtering, which functioned as both a physical passivation barrier and a hole-transferring catalyst for water oxidation (**Figure 6**a).[59] Note that the surface of Ni was gradually converted to nickel oxide. The photoanode exhibited a photocurrent density of over 10 mA/cm^2 in 0.1 M Na_2S at 0 V vs. Ag/AgCl under AM 1.5G simulated sunlight at 100 mW/cm^2. However, the photocurrent of the photoanode could be maintained above 2 mA/cm^2 for only 15-20 min. Wang et al. applied this ultrathin Ni passivation strategy to their surface-functionalized $MAPbI_3$ and further improved the stability to approximately 30 min, but the photocurrent density was reduced to 2.1 mA/cm^2.[62] Building on this layered structure with Ni as the protective and catalytic layer, in 2016, Hoang et al. further use a dense hole-transport layer ~~modified the hole transport layer to be pinhole-free~~ to enhance the stability of the $MAPbI_3$ photoelectrode.[63] The device stability was increased from 15 min to more than 30 min. Later, in 2018, Nam et al. have fabricated a more stable $MAPbI_3$ photoanode by introducing a low-

melting-point Field's metal layer between the perovskite and Ni layers.[64] The perovskite photoanode was found to be stable for 6 hours at approximately 13 mA/cm^2 under 0.7 Sun illumination and a bias of 1.3 V vs. RHE in KOH solution.

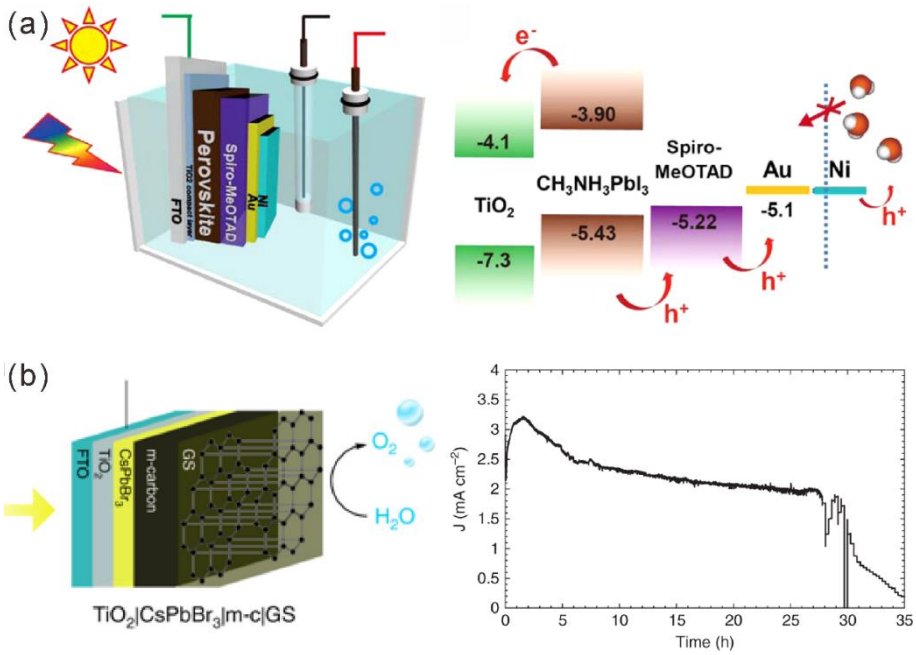

Figure 6. (a) Schematic illustration of photoelectrochemical test of a Ni-coated perovskite photoanode in a standard three-electrode system. The panel on the right shows the schematic energy diagram of the photoelectrode. Reprinted with permission from Ref.[59] Copyright 2015, American Chemical Society. (b) Schematic illustration of the $CsPbBr_3$ photoanode for O_2 evolution. The panel on the right shows the current density as a measure of the stability of the photoanode in water. Reprinted with permission from Ref.[61] Copyright 2019, Nature Publishing Group.

Carbon materials have also been employed as protective layers for halide perovskites. Tao et al. encapsulated a $(5\text{-AVA})_x(MA)_{1-x}PbI_3$ [5-AVA = $HOOC(CH_2)_4NH_3^+$]-based photoanode with conductive carbon paste and silver conductive paint for water oxidation.[65] The photoanode achieved unprecedented stability, remaining stable in an alkaline electrolyte for more than 48 h. The material also showed a high photocurrent density of 12.4 mA/cm^2 at 1.23

V vs. RHE in an alkaline electrolyte. This high stability was largely due to the coating of a thick carbon layer (several hundreds of μm) onto the halide perovskites (did they detect or monitored CO and CO2?). Very recently, Poli et al. used a commercial thermal graphite sheet and a mesoporous carbon scaffold to encapsulate a $CsPbBr_3$-based photoanode (Figure 6b).[61] A record stability of 30 h in aqueous electrolyte with current above 2 mA/cm^2 at 1.23 vs. RHE was achieved under constant simulated solar illumination. Furthermore, by functionalizing the surface of the graphite sheet with an Ir-based water oxidation catalyst, the onset potential of the composite photoanode was cathodically shifted by 100 mV. Notably, ~ 9 μmol of evolved O_2 were detected over a ~ 130 min test using their TiO_2|$CsPbBr_3$|m-c|GS|WOC photoelectrode under continuous simulated solar light irradiation (AM 1.5 G, 100 mW/cm^2), in 0.1M KNO_3 adjusted to pH 3.5 with H_2SO_4. This achievement marks by far the most stable and efficient halide perovskite photoanode for water oxidation.

3.2.Water reduction

Field's metal (a eutectic In-Bi-Sn alloy) is the most widely used protective and conductive layer since its first demonstration by the Reisner group as a coating for a $MAPbI_3$-based photocathode for water reduction (**Figure 7**a).[36] With Pt nanoparticles loaded as the hydrogen evolution electrocatalysts, the Reisner group obtained a record photocurrent density of 9.8 mA/cm^2 at 0 V vs. RHE with an onset potential of 0.95 ± 0.03 vs. RHE. The photoelectrode showed high stability, retaining more than 80% of its initial photocurrent for ~ 1 h under continuous illumination (100 mW/cm^2, AM 1.5 G, λ > 400 nm). The group further fabricated a tandem PEC system by coupling a Field's metal-protected cesium formamidinium methylammonium (CsFAMA) triple cation mixed halide perovskite photocathode with a stable $BiVO_4$ | TiCo photoanode for bias-free solar-to-hydrogen (STH) production (Figure 7b).[66] The perovskite photocathode alone could operate for up to 7 h with a photocurrent density of 12.1 ± 0.3 mA/cm^2 at 0 V vs. RHE. After coupling with a $BiVO_4$ photoanode, the PEC tandem system, with a

device surface area of 0.25 cm^2, could operate for up to 20 h with a bias-free STH efficiency of 0.35 ± 0.14%. Remarkably, by virtue of the high reliability of the fabrication procedures, the tandem device could be scaled up to 10 cm^2 with only a slight drop in the photocurrent density. Also using Field's metal as the protective layer, Gao et al. fabricated an all-inorganic photocathode by incorporating $CsPbBr_3$ as the perovskite layer and NiO and ZnO as the hole and electron transport layers, respectively.[67] This all-inorganic photocathode achieved a photocurrent of approximately 1.2 mA/cm^2 at 0 V vs. RHE and retained approximately 94% of its initial photocurrent after continuous illumination for 1 h (AM 1.5G).

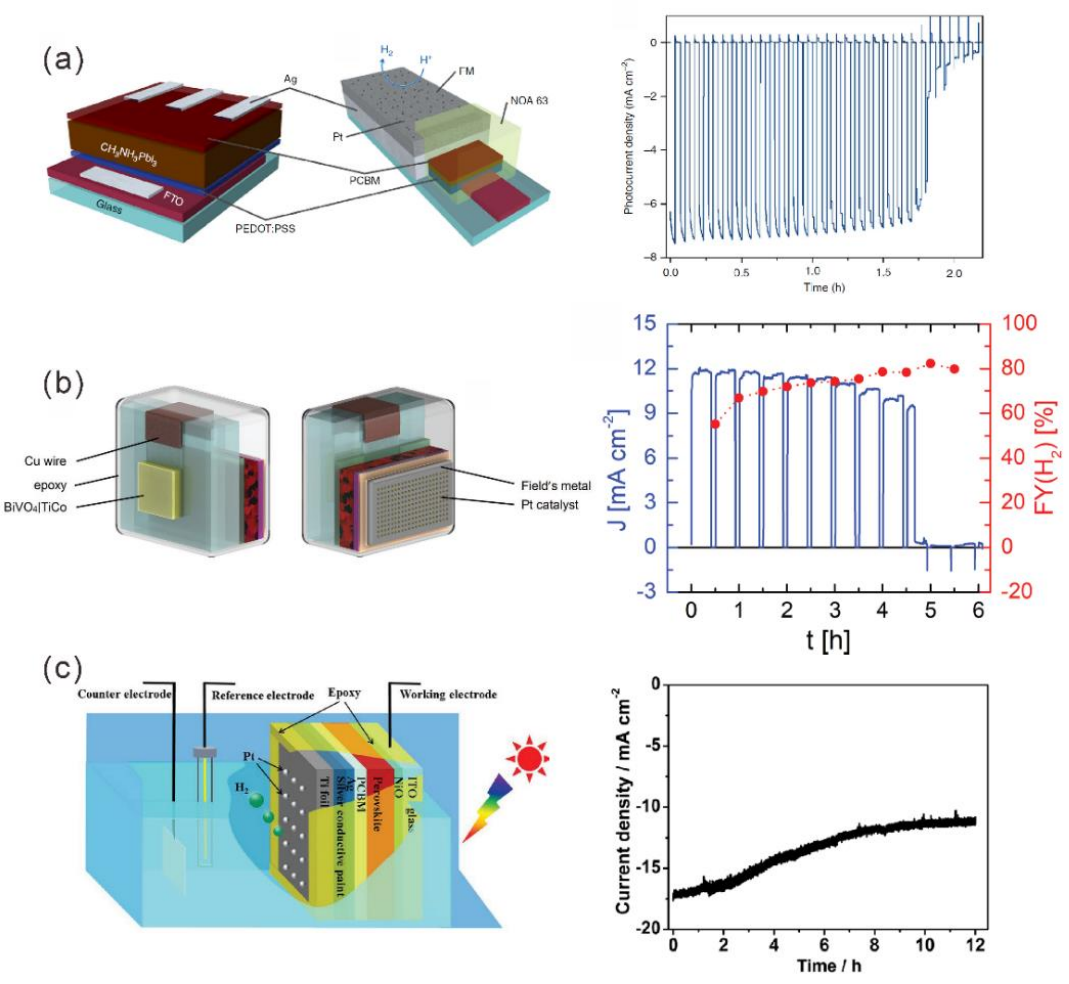

Figure 7. (a) Schematic illustration of a perovskite solar cell and the photocathode built upon it with a Field's metal encapsulating layer. The panel on the right shows the chronoamperometric trace recorded at an applied potential of 0 V vs. RHE. Reprinted with

permission from Ref.[36] Copyright 2016, Nature Publishing Group. (b) Skewed views of the PEC tandem cell showing the $BiVO_4$ photoanode on the front and the perovskite photocathode with Field's metal encapsulation on the back. The panel on the right shows the current density at 0 V vs. RHE and the corresponding faradaic yield. Reprinted with permission from Ref.[66] Copyright 2018, Wiley. (c) Schematic illustration of the Ti foil-protected $MAPbI_3$ photocathode for PEC H_2 evolution in a three-electrode system. The panel on the right shows the chronoamperometry (current density) curve of Pt-Ti/$MAPbI_3$ photocathode 0 V vs. RHE. Reprinted with permission from Ref.[60] Copyright 2018, Wiley.

Titanium foil is another good choice for protecting halide perovskite photoelectrodes. Zhang et al. fabricated a sandwich-like structure by pasting Ti foil onto a $MAPbI_3$-based photocathode (Figure 7c).[60] With Pt loaded as the catalyst, this photocathode exhibited an onset potential at 0.95 V vs. RHE and a photocurrent density of 18 mA/cm^2 at 0 V vs. RHE, with an ideal ratiometric power-saved efficiency of 7.63%. Impressively, the photocathode retained good stability under 12 h of continuous illumination in water over a wide pH range.

3.3.CO_2 reduction

One aim of CO_2 reduction via photoelectrocatalysis is to alleviate the energy crisis and environmental issues by producing C_1-C_3 chemical fuels. The products of CO_2 reduction in aqueous media can be mixtures of formic acid, carbon monoxide, formaldehyde, methane and C_2-C_3 hydrocarbons. In this context, the goal of CO_2 reduction is to efficiently, stably and selectively produce a target product. Thermodynamically, halide perovskites can drive CO_2 reduction reactions because they generally possess sufficiently negative conduction band potentials (Figure 1). However, CO_2 reduction using a halide perovskite-based photoelectrode has scarcely been reported. Encouragingly, Chen *et al.* recently demonstrated In-Bi alloy-coated $MAPbI_3$-based photocathodes for selective CO_2 reduction with nearly 100% FE for formic acid production in aqueous solution (**Figure 8**a).[37] The $In_{0.4}Bi_{0.6}$ composition was identified by a

compositional screening strategy of a ternary In-Bi-Sn low melting-point alloy system. The photocathode was then fabricated by coating the catalytic, protective, and conductive $In_{0.4}Bi_{0.6}$ alloy layer onto the halide perovskite. The photocathode operated at -0.6 V vs. RHE under simulated AM 1.5G irradiation for more than 1.5 h (Figure 8b) and achieved a photo-assisted electrolysis system efficiency of 7.2%.

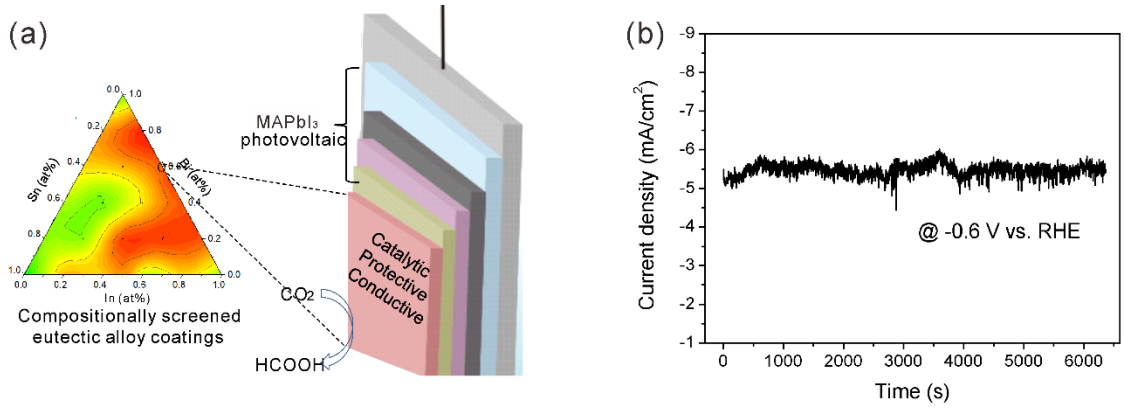

Figure 8. (a) Schematic illustration of the compositional screening and photoelectrode structure of **? (b) Stability of the photocathode under irradiation at -0.6 V vs. RHE under AM 1.5G irradiation. Reprinted with permission from Ref.[37] Copyright 2019, American Chemical Society.

Studies detailing the use of halide perovskite-based photoelectrodes for water splitting and CO_2 reduction are summarized in **Table 2**. As indicated, the as-developed halide perovskite photoelectrodes generally exhibit better stability than the photocatalysts, as the well-defined perovskite layers are well protected in the photoelectrodes. The overall performance (including stability and efficiency) of the photoelectrodes is quite promising, with the $CsPbBr_3$ | mesoporous carbon | graphite sheet | Ir OER and $(CsMAFA)PbI_xBr_{3-x}$ | FM | Pt–$BiVO_4$ | TiCo designs considered the best for water oxidation and reduction, respectively. However, photoelectrodes for CO_2 reduction have been rarely reported; only work on the $MAPbI_3$ | $In_{0.4}Bi_{0.6}$ structure has been published. We believe that there is much more to be done regarding

water splitting and selective CO_2 reduction to a target chemical fuel using halide perovskite photoelectrodes.

Table 2. A summary of the reported photoelectrodes using halide perovskites. FM: Field's metal; FE: faradaic efficiency; STH: solar-to-hydrogen efficiency.

Photoelectrode	Reaction	Electrolyte	Light source	Stability	Efficiency	Ref.
$MAPbI_3$ | Ni	H_2O Ox.	0.1 M Na_2S	100 mW/cm^2, AM 1.5 G	15-20 min	10 mA/cm^2 @ 0 V vs. Ag/AgCl	[59]
Surface-functionalized $MAPbI_3$ | Ni	H_2O Ox.	0.1 M Na_2S	100 mW/cm^2, AM 1.5 G	> 30 min	2.1 mA/cm^2 @ 0 V vs. Ag/AgCl	[62]
$MAPbI_3$ | pinhole-free HTL | Ni	H_2O Ox.	Not clear	Simulated illumination (0.7 Sun)	> 30 min	17.4 mA/cm^2 @ 1.23 V vs. SHE	[63]
$MAPbI_3$ | FM | Ni	H_2O Ox.	1.0 M KOH solution	Simulated illumination (0.7 Sun)	6 h	13 mA/cm^2 @ 1.3 V vs. RHE	[64]
$(5\text{-AVA})_x(MA)_{1-x}PbI_3$ | conductive carbon paste	H_2O Ox. [a)]	1.0 M KOH solution	100 mW/cm^2, AM 1.5 G	> 48 h	12.4 mA/cm^2 @ 1.23 V vs. RHE	[65]

$CsPbBr_3$ | mesoporous carbon | graphite sheet | Ir OER	H_2O Ox. [a)]	0.1 M KNO_3	100 mW/cm^2, AM 1.5 G	30 h	2 mA/cm^2 @ 1.23 V vs. RHE	[61]
$MAPbI_3$ | FM | Pt	H_2O Red.	0.1M borate	100 mW/cm^2, AM 1.5 G, λ > 400 nm	> 1 h	9.8 mA/cm^2 @ 0 V vs. RHE; FE ~ 95%	[36]
(CsMAFA)PbI_xBr_{3-x} | FM | Pt–$BiVO_4$ | TiCo (0.25 cm^2)	H_2O Red.	0.1M borate, K_2SO_4	100 mW/cm^2, AM 1.5 G	18 h	~0.39 mA/cm^2 (no-bias); STH ~ 0.35%	[66]
(CsMAFA)PbI_xBr_{3-x} | FM | Pt–$BiVO_4$ | TiCo (10 cm^2)	H_2O Red.	0.1M borate, K_2SO_4	100 mW/cm^2, AM 1.5 G	14 h	~0.23 mA/cm^2 (no-bias); STH ~ 0.15%	[66]
$CsPbBr_3$ | FM | Pt	H_2O Red.	0.2 M Na_2HPO_4/NaH_2PO_4	100 mW/cm^2, AM 1.5 G	> 1 h	1.2 mA/cm^2 @ 0 V vs. RHE.	[67]
$MAPbI_3$ | Ti foil | Pt	H_2O Red.	0.5 M H_2SO_4	100 mW/cm^2, AM 1.5 G	12 h	18 mA/cm_2 @ 0 V vs. RHE. Ideal ratiometric	[60]

					power-saved efficiency of 7.63%.	
$MAPbI_3$ | $In_{0.4}Bi_{0.6}$	CO_2 Red.	0.1 M $KHCO_3$	100 mW/cm^2, AM 1.5G	> 1.5 h	~5.2 mA/cm$_2$ @ -0.6 V vs. RHE. photo-assisted electrocatalysis efficiency of 7.2%.	[37]

[a)]Oxygen was measured and quantified in these works.

4. Perovskite Photovoltaics Integrated with (Photo)electrocatalysis

Halide perovskite photovoltaics (PVs) can be aligned with a photoelectrode for wide-spectrum solar-chemical fuel conversion or can act as an external circuit to power an electrocatalytic cell. A simplified illustration of a PV-integrated (photo)electrocatalytic system is shown in **Figure 9**, in which the PV absorbs light and provides the needed photovoltage for the both cathodic and anodic reactions to occur.

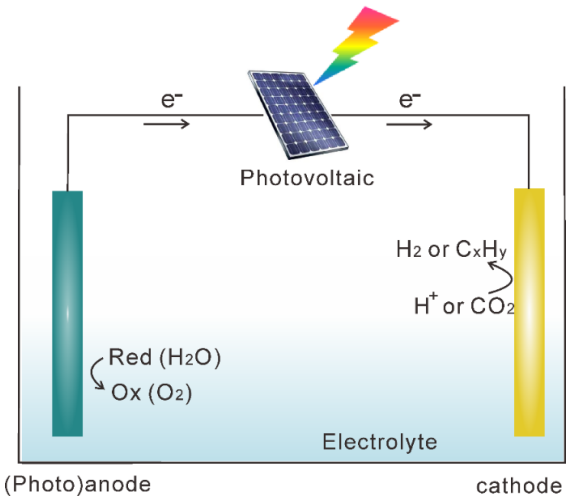

Figure 9. An illustration of a photovoltaic-integrated (photo)electrocatalysis system. The anode can be (or can also be?) photoactive.

In a PV-PEC (where the electrodes are photo-active) or PV-EC system, the halide perovskite PV is isolated from the solution, acting as the photovoltaic power source for an unbiased solar-chemical fuel conversion device. Halide perovskite PVs generally have large open-circuit voltages (1 - 1.4 eV). Therefore, two halide perovskite PV cells in tandem are enough to drive overall water splitting, whereas three cells in tandem are needed when using conventional Si and CIGS PVs. In addition, the cost of solution-processable halide perovskite PVs is much lower than that of Si or CIGS cells. In the following, we discuss the progress made in the development of PV-(photo)electrocatalysis systems.

4.1.Photovoltaic integrated with photoelectrocatalysis

In an integrated PV-PEC system, a photoanode or photocathode is connected in series to a halide perovskite PV. The photoanode(cathode) is often stacked on top of the halide perovskite PV because of its larger band gap (> 2 eV) than that of the halide perovskite. $BiVO_4$ is the most well-studied photoanode for water oxidation due to its suitable band gap (2.4 eV) and superior PEC performance. In 2015, Kamat group demonstrated an all-solution-processed tandem water-splitting device composed of a cobalt phosphate (CoPi) catalyst-modified $BiVO_4$ photoanode

and a single-junction $MAPbI_3$ perovskite solar cell.[68] As shown in **Figure 10**a, the perovskite solar cell is placed under the $BiVO_4$ photoanode so that wavelengths > 500 nm can pass through the $BiVO_4$ photoanode. This configuration allows for efficient solar photon management, with the metal oxide photoanode selectively harvesting high-energy visible photons and the underlying perovskite solar cell capturing lower-energy visible-near IR wavelengths in a single-pass excitation. Therefore, to make full use of the lower-energy light in the bottom layer, the top layer should be highly transparent (Figure 10b, with $BiVO_4$ as the top layer). Because two modules are connected in series, the operating photocurrent density of a tandem PV-photoanode device can be predicted from the intersection of the individual J-V curves (Figure 10c). This PV-photoanode device exhibited a STH efficiency of 2.5% at neutral pH without external bias (Figure 10d). Kim et al. applied a dual-doping strategy (hydrogen treatment and 3 at% Mo doping) to modify the $BiVO_4$ photoanode and then loaded cobalt carbonate (Co-Ci) as a catalyst. They further fabricated a $MAPbI_3$ PV-$BiVO_4$ photoanode tandem device with a STH efficiency of 4.3% in the wired configuration and 3.0% in the wireless configuration for a long stability test (12 h).[69] Fe_2O_3 is another widely studied photoanode for halide perovskite PV-PEC tandem devices. Gurudayal et al. demonstrated that a $MAPbI_3$ solar cell in tandem with a Fe_2O_3 photoanode can achieve overall water splitting with a STH efficiency of 2.4%.[70] Other photoanodes such as TiO_2, CdS, $BiVO_4/WO_3$ and $BiVO_4/WO_3/SnO_2$ have also been integrated with halide perovskite solar cells, as summarized in Table 3. In addition to photoanodes, photocathodes have also been used in tandem devices with halide perovskite PVs. Mayer group fabricated a tandem device using a Cu_2O as the photoanode and a $FA_xMA_{1-x}PbI_3$ solar cell connected to an IrO_2 as the anode.[71] This device yield a STH of 2.5% for unbiased water splitting.

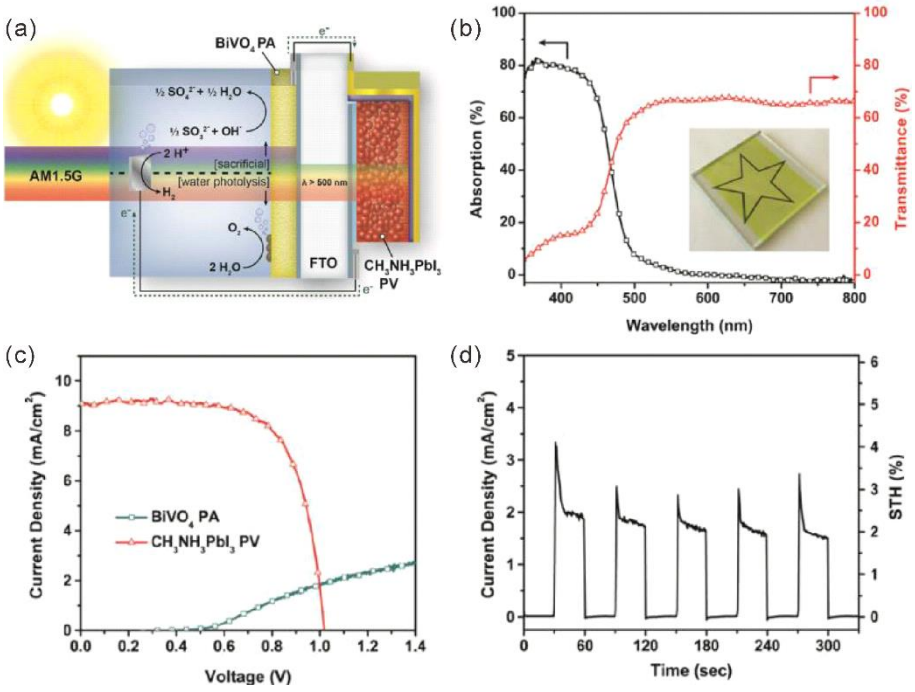

Figure 10. (a) Schematic diagram of a tandem $MAPbI_3$ PV-$BiVO_4$ device for solar fuel generation. (b) Optical absorption and transmittance of the $BiVO_4$ thin film. Inset: photograph demonstrating the translucence and limited visible-light scattering of the spin-cast $BiVO_4$ thin film. (c) Overlaid J-V characteristics of CoPi/$BiVO_4$ photoanode and $MAPbI_3$ solar cell. The photovoltaic parameters were recorded through a CoPi/$BiVO_4$ film. CoPi/$BiVO_4$ was measured in a three-electrode configuration with an Ag/AgCl reference electrode and a Pt counter electrode. The crossing point of the two curves designates the anticipated photocurrent output of the series-connected tandem device. (d) Photocurrent density and calculated STH efficiency as a function of time for the $MAPbI_3$-CoPi/$BiVO_4$ device, demonstrating the ability to drive neutral water oxidation and reduction at 2.5% efficiency without external bias. All figures are reprinted with permission from Ref.[68] Copyright 2015, American Chemical Society.

As summarized in **Table 3**, most halide perovskite solar cells incorporated into PV-PEC tandem devices are based on $MAPbI_3$ because of the material's relatively small band gap (~1.55 eV). However, one of the most important advantages of halide perovskites is their band-gap tunability (1.1-2.3 eV), which can lead to compatibility with a wide variety of photoelectrodes.

Recently, cation (Cs^+, FA^+ and MA^+) and anion (Br^- and I^-) mixed halide perovskites have been demonstrated to have large open-circuit voltages and good stability, resulting in excellent tandem device performance when integrated with a Mo:$BiVO_4$ photoanode.[72] In addition, Luo et al. fabricated a large-band-gap perovskite $MAPbBr_3$ (E_g = 2.3 eV) PV-photocathode tandem device, in which the photocathode was made of small-band-gap $CuIn_xGa_{1-x}Se_2$ (1.1 eV).[73] Therefore, the halide perovskite solar cell was stacked on top of the photocathode. This tandem device yielded a high STH of ~6%.

One of the key requirements of a PV-PEC tandem device is that the top layer with larger band gap should be highly transparent. One way to meet this requirement when using an opaque photoanode(cathode) is to use a beam splitter to separate the solar spectrum into two light beams, which will be irradiated onto the photoanode(cathode) and solar cell separately.[72, 74] Another key issue is the significant energy loss due to the mismatch between the photocurrent of the wide-band-gap photoanode(cathode) and that of the narrow-band-gap solar cell (Figure 10c). Therefore, further improving the current of the photoanode(cathode) to make it compatible with that of the solar cell is crucial for improving the STH efficiency. To this end, the Sharp group has demonstrated a new three-terminal cell design in which a second junction is added to extract charge carriers that cannot be injected into the top junction due to current mismatch.[75] This concept may be applied to halide perovskite PV-PEC tandem devices in the future.

Unlike the vastly reported study of water splitting, the study of CO_2 reduction using a PV-PEC tandem device is so far rarely reported. Jang et al. reported CO_2-to-CO conversion using a $MAPbI_3$ PV-ZnO@ZnTe@CdTe core-shell nanorod array photocathode in tandem.[76] With solar energy as the only energy source, this tandem device achieved a solar-to-CO conversion efficiency of 0.35%.

Table 3. Summary of reported halide perovskites photovoltaics integrated with photoelectrocatalysis systems for water splitting. STH: solar-to-hydrogen conversion efficiency. BVO: $BiVO_4$.

Photovoltaic	Photoanode	Area (cm^2)	Electrolyte	Stability	STH	Ref.
$MAPbI_3$	TiO_2@BVO	/	0.1 M PBS	0.8 h	1.24%[a)]	[77]
$MAPbI_3$	CoPi/BVO	0.54	0.1 M KPi	5 min	2.5%	[68]
$MAPbI_3$	Co-Ci/Mo:BVO	0.45	0.1 M KCl	12 h	4.3% (wired); 3% (wireless)[a)]	[69]
$MAPbI_3$	CoPi/Mn:Fe_2O_3	0.12	1 M NaOH	8h	2.4%[a)]	[70]
$MAPbI_3$	Sn:TiO_2	0.13	1 M KOH	2 h	1.5%	[78]
$MAPbI_3$	NiOOH/FeOOH/BVO/WO_3	0.5	0.5 M KPi	1 h	~3.3%	[79]
$MAPbI_3$	CoPi/Sn:Fe_2O_3	0.12	1 M NaOH	120 s	3.4%	[80]
$MAPbI_3$	CoO_x/BVO/WO_3/SnO_2	0.196	0.5 M KPi	15 min	4.5%[a)]	[81]
$Cs_{0.05}(FA_{0.83}MA_{0.17})_{0.95}Pb(I_{0.83}Br_{0.17})_3$	NiOOH/FeOOH/BVO	/	1 M KBi	10 h	6.5%[a)]	[82]
$MAPbI_3$	CdS/TiO_2	1	0.1 M NaOH	1 h	1.54%	[83]
$MAPbI_3$	NiOOH/FeOOH/ Mo: BVO	0.25	0.5 M KPi	10 h	6.2%[a)]	[74]
$FA_{0.83}Cs_{0.17}PbI_2Br$	NiOOH/FeOOH/ Mo: BVO	0.25	0.5 M KPi	6 h	6.3%[a)]	[72]
CIGS (photocathode)	$MAPbBr_3$/DSA	0.16	0.5 M H_2SO_4	180 s	6%	[73]

Cu_2O (photocathode)	$FA_xMA_{1-x}PbI_3/IrO_2$	0.057	0.5 M Na_2SO_4, 0.1 M NaPi	2 h	2.5%[a)]	[71]

[a)]Oxygen was measured and quantified in these works.

4.2.Photovoltaics integrated with electrocatalysis

Perovskite solar cells can serve as separate and external power sources to generate sufficiently high voltages to drive electrocatalysis. Grätzel and co-workers were first to demonstrate that two perovskite solar cells in tandem could power overall water splitting (**Figure 11**).[8] More specifically, they used a $MAPbI_3$-based solar cell with a short-circuit photocurrent density (J_{sc}), open-circuit voltage (V_{oc}), fill factor and PCE of 21.3 mA/cm^2, 1.06 V, 0.76 and 17.3%, respectively. The electrocatalysts for both water reduction and oxidation were earth-abundant and robust NiFe layered double hydroxides (LDHs), which only required 1.7 V across the electrodes to achieve a 10 mA/cm^2 water-splitting current in a 1 M NaOH aqueous electrolyte. Then, an overall water-splitting cell was assembled by connecting two $MAPbI_3$ solar cells (a tandem cell) to the NiFe LDH electrodes (**Figure 11**a-b). The tandem cell exhibited a J-V response with a V_{oc} of 2.00 V and a PCE of 15.7%, as depicted in Figure 11c. The authors predicted the operating current density of the integrated system (normalized to the total illuminated area of the solar cells) by defining the intersection of the J-V curves of the tandem cell and the catalyst electrodes in the two-electrode configuration as the operating point. At this point, an operating current density of 10 mA/cm^2 and STH of 12.3% can be obtained. This operating point of the water-splitting cell occurs very close to the maximum power point of the perovskite tandem cell (9.61 mA/cm^2 at 1.63 V, PCE 15.7%), indicating that minimal energy is lost in converting electrical to chemical energy in this system. The authors further measured the current density in the standalone, unbiased light-driven configuration to confirm that the system indeed operated at 10 mA/cm^2 with a STH of 12.3% (Figure 11d).

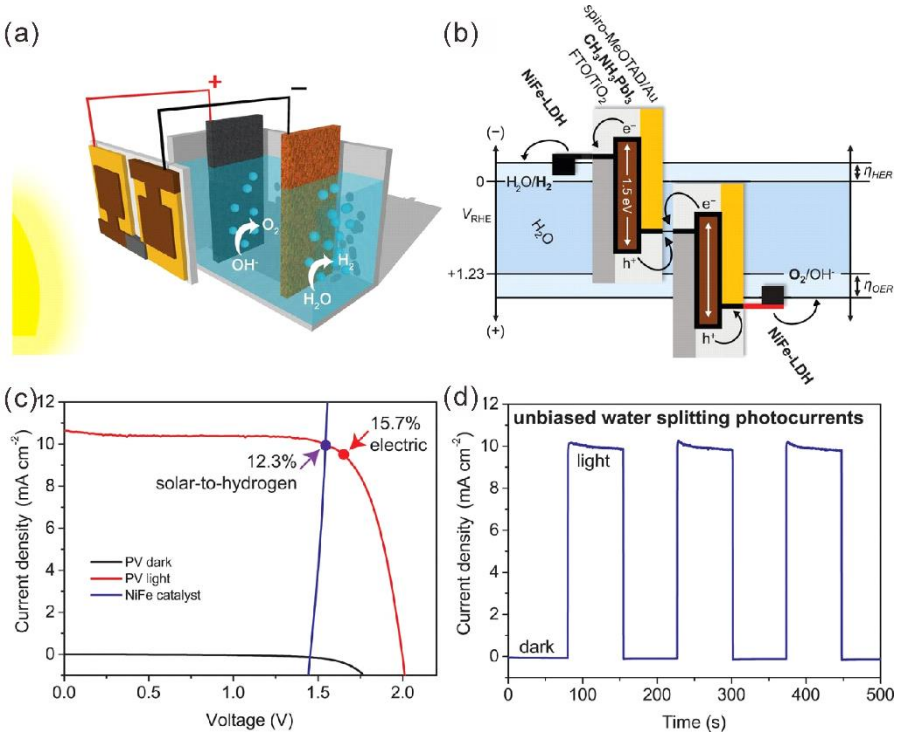

Figure 11. (a) Schematic diagram of a water-splitting device. (b) A generalized energy schematic of the perovskite tandem cell for water splitting. (c) J-V curves of the perovskite tandem cell in the dark and under simulated illumination (100 mW/cm^2, AM 1.5G) and of the NiFe layered double hydroxides (LDH) electrodes in a two-electrode configuration. (d) Current density-time profile of the integrated water-splitting device without external bias under a chopped simulated illumination (100 mW/cm^2, AM 1.5G). All figures were reprinted with permission from Ref.[8] Copyright 2014, AAAS.

One of the drawbacks of this PV-electrocatalysis design is that the electrocatalyst for both water oxidation and water reduction in the same solution is very limited. In this regard, Grätzel et al. modified their electrocatalytic cell by separating the anode half-cell and cathode half-cell using a bipolar membrane.[84] With this approach, the authors were able to expand the selection of a H_2 evolution catalyst in acid solution and an O_2 evolution catalyst in alkaline solution. Specifically, the authors selected CoP as the H_2 evolution catalyst in 0.5 M H_2SO_4 and NiFe LDH as the O_2 evolution catalyst in 1 M KOH. This cell only required 1.63 V to achieve a

photocurrent density of 10 mA/cm^2. Thus, a high STH conversion efficiency of 12.7% was achieved upon the integration of the perovskite PV cell with the newly designed electrocatalytic cell.

The Grätzel group also applied this integrated PV-EC structure to reduce CO_2 to CO.[85] Three $MAPbI_3$ solar cells were connected in tandem to serve as a power source with a V_{oc} of 3.1 V, J_{sc} of 6.15 mA/cm^2 and PCE of 13.4%. Au and IrO_2 were selected as the electrocatalysts for CO_2 reduction and water oxidation at the cathode and anode ends, respectively. Powering this Au-IrO_2 electrocatalytic cell requires a driving voltage of at least 2 V, considering the thermodynamic voltage ($CO_2 \rightleftharpoons CO + 1/2O_2$; ΔE = 1.34 V) and the overpotentials for the two electrodes (300 mV on the cathode Au, 400 mV on the anode IrO_2). The perovskite tandem cell was then integrated with the electrocatalytic cell to form a PV-electrocatalysis cell, operated at 5.8 mA/cm^2 for at least 18 hours with a solar-to-CO efficiency exceeding 6.5%. This work represents a benchmark in sunlight-driven CO_2 conversion.

5. Conclusion and Prospects

Considerable effort has been devoted to studying different aspects of solar to fuel conversions. While progress has been made in particular in the last two decades, the slow reaction rates, the lack of stable material in aqueous environment and the low energy density of sun light on earth surface (1 kW/m^2), some of the daunting challenges at present, have been identified to be among the key limiting factors . The complexity of the multi-component photocatalysts and the nature of reaction media (aqueous environment) limit diffraction and electron spectroscopy-based techniques required for investigations. Halide perovskites are recently discovered semiconductors with remarkable photophysical properties and great promises to achieve efficient solar fuel conversion. To date, various halide perovskite photocatalysts, photoelectrodes and reaction system configurations have been designed, studied, tested and further improved. For instance, H_2 can be produced from HI using $MAPbI_3$

photocatalysts; photocatalytic CO_2 reduction can be achieved in ethyl acetate with $CsPbBr_3$ photocatalysts; and $MAPbI_3$ can be used as a photocathode or photoanode for reduction and oxidation reactions, respectively. Moreover, $MAPbI_3$ photovoltaics can be integrated with photoelectrocatalytic or electrocatalytic cells for bias-free water splitting or CO_2 reduction. Nevertheless, despite the great efforts and achievements summarized above, there is still much room for improvement in developing halide perovskite materials and in designing solar-chemical fuel conversion systems to enhance stability, efficiency and environmental friendliness for future practical applications. Several possible directions and the associated challenges for further research are suggested in the following.

1) Functional perovskite@shell core-shell structures need to be further explored. A semi-conductive or conducive shell may well encapsulate a perovskite core for use in aqueous medium facilitating charge carrier transfer via interfacial or band-alignment engineering across the core-shell structures. Further functionalization of the shells with nanoparticles or ligands will enable more efficient solar-fuel conversion and even a wider scope of photocatalytic applications beyond water splitting and CO_2 reduction. However, construction of perovskite@shell structures remains challenging, largely because the solvents for halide perovskite growth are usually incompatible with the solvents for shell formation.

2) New protective layers should be established by developing advanced coating techniques and expanding the choice of protective layers. Coating halide perovskite photoelectrodes or photovoltaics with a protective and conductive layer while technically pragmatic,the strategy currently undertaken has higher engineering component than scientific. For that, methodology for operando study during and after the protective layer deposition are needed. Such studies may include operando X-ray absorption spectroscopy, materials testing following epitaxy deposition, and core and valence level spectroscopy are all available techniques that can be used.

3) More attention could be paid to halide perovskite nanostructures. Halide perovskite nanostructures exhibit enhanced structural and chemical stability due to surface effects compared to their bulk forms. Because nanostructures have a high surface-area-to-volume ratio, the effect of surface reactivity on the chemical properties and phase stability of nanostructures becomes significant. Moreover, nanostructure design could help us understand the dynamics between surface and bulk, the semiconductor-metal interface and structure-sensitive effects on charge transfer, leading to active and stable catalysts with enriched surface-active sites.

4) The design of the reaction solution and the tandem device configuration needs further optimization. Regarding the solution system, exploration of viable solutions for halide perovskites in conjunction with targeting reactions beyond water splitting or CO_2 reduction. For example, redox flow batteries based on halide perovskite would be feasible once suitable redox couples and solution systems are established. Regarding tandem devices, there are still problems to be solved, such as current mismatch, opaque top layers and large series resistance. Concerted efforts are needed from researchers in fields such as optoelectronic devices, materials synthesis and catalysis.

5)More attention to the development of lead-free halide perovskites is needed. Most of today's high-performance photocatalysts and devices are based on lead halide perovskites; however, the toxicity of lead creates serious environmental concern. In this regard, tin-based and double halide perovskites[86] with comparable photophysical properties could be explored as alternatives.

In summary, tremendous efforts have been made to enable halide perovskites to act as catalysts or part of catalytic systems needed for solar-to-chemical fuel conversion. In this review, we have summarized and discussed strategies established for fabricating halide perovskites for utilization in photocatalytic particle-suspension systems, photoelectrode thin-film systems and photovoltaic-(photo)electrocatalytic tandem systems that target water splitting, HI splitting, and CO_2 reduction reactions. The future of halide perovskites in those

applications is promising but will depend on discovering new and stable perovskite materials; developing protective and functional shells and layers; and designing suitable reaction solution systems as well as tandem device configurations.

Acknowledgements

This work was supported by King Abdullah University of Science and Technology (KAUST).

Received: ((will be filled in by the editorial staff))
Revised: ((will be filled in by the editorial staff))
Published online: ((will be filled in by the editorial staff))

References

[1] P. De Luna, C. Hahn, D. Higgins, S. A. Jaffer, T. F. Jaramillo, E. H. Sargent, *Science* **2019**, *364*.
[2] X. Chen, S. Shen, L. Guo, S. S. Mao, *Chem. Rev.* **2010**, *110*, 6503.
[3] S. Shen, J. Chen, M. Wang, X. Sheng, X. Chen, X. Feng, S. S. Mao, *Prog. Mater. Sci.* **2018**, *98*, 299.
[4] K. Sun, S. Shen, Y. Liang, P. E. Burrows, S. S. Mao, D. Wang, *Chem. Rev.* **2014**, *114*, 8662.
[5] J. L. White, M. F. Baruch, J. E. Pander Iii, Y. Hu, I. C. Fortmeyer, J. E. Park, T. Zhang, K. Liao, J. Gu, Y. Yan, T. W. Shaw, E. Abelev, A. B. Bocarsly, *Chem. Rev.* **2015**, *115*, 12888.
[6] O. S. Bushuyev, P. De Luna, C. T. Dinh, L. Tao, G. Saur, J. van de Lagemaat, S. O. Kelley, E. H. Sargent, *Joule* **2018**, *2*, 825.
[7] N. Zhang, R. Long, C. Gao, Y. Xiong, *Sci. China Mater.* **2018**, *61*, 771.
[8] J. Luo, J.-H. Im, M. T. Mayer, M. Schreier, M. K. Nazeeruddin, N.-G. Park, S. D. Tilley, H. J. Fan, M. Grätzel, *Science* **2014**, *345*, 1593.
[9] C.-T. Dinh, T. Burdyny, M. G. Kibria, A. Seifitokaldani, C. M. Gabardo, F. P. García de Arquer, A. Kiani, J. P. Edwards, P. De Luna, O. S. Bushuyev, C. Zou, R. Quintero-Bermudez, Y. Pang, D. Sinton, E. H. Sargent, *Science* **2018**, *360*, 783.
[10] K. Sivula, R. van de Krol, *Nat. Rev. Mater.* **2016**, *1*.
[11] P. V. Kamat, *Acc. Chem. Res.* **2017**, *50*, 527.
[12] A. Kojima, K. Teshima, Y. Shirai, T. Miyasaka, *Journal of the American Chemical Society* **2009**, *131*, 6050.
[13] D. Shi, V. Adinolfi, R. Comin, M. Yuan, E. Alarousu, A. Buin, Y. Chen, S. Hoogland, A. Rothenberger, K. Katsiev, Y. Losovyj, X. Zhang, P. A. Dowben, O. F. Mohammed, E. H. Sargent, O. M. Bakr, *Science* **2015**, *347*, 519.
[14] Y. Yang, Y. Yan, M. Yang, S. Choi, K. Zhu, J. M. Luther, M. C. Beard, *Nature communications* **2015**, *6*, 7961.
[15] G. Xing, N. Mathews, S. Sun, S. S. Lim, Y. M. Lam, M. Grätzel, S. Mhaisalkar, T. C. Sum, *Science* **2013**, *342*, 344.
[16] A. A. Zhumekenov, M. I. Saidaminov, M. A. Haque, E. Alarousu, S. P. Sarmah, B. Murali, I. Dursun, X.-H. Miao, A. L. Abdelhady, T. Wu, O. F. Mohammed, O. M. Bakr, *ACS Energy Lett.* **2016**, *1*, 32.
[17] E. Alarousu, A. M. El-Zohry, J. Yin, A. A. Zhumekenov, C. Yang, E. Alhabshi, I. Gereige, A. AlSaggaf, A. V. Malko, O. M. Bakr, O. F. Mohammed, *The journal of physical chemistry letters* **2017**, *8*, 4386.
[18] J. Liu, K. Song, Y. Shin, X. Liu, J. Chen, K. X. Yao, J. Pan, C. Yang, J. Yin, L.-J. Xu, H. Yang, A. M. El-Zohry, B. Xin, S. Mitra, M. N. Hedhili, I. S. Roqan, O. F. Mohammed, Y. Han, O. M. Bakr, *Chemistry of Materials* **2019**.
[19] S. De Wolf, J. Holovsky, S. J. Moon, P. Loper, B. Niesen, M. Ledinsky, F. J. Haug, J. H. Yum, C. Ballif, *The journal of physical chemistry letters* **2014**, *5*, 1035.
[20] Y. Fu, H. Zhu, J. Chen, M. P. Hautzinger, X. Y. Zhu, S. Jin, *Nat. Rev. Mater.* **2019**, *4*, 169.
[21] M. V. Kovalenko, L. Protesescu, M. I. Bodnarchuk, *Science* **2017**, *358*, 745.
[22] Y. Fu, F. Meng, M. B. Rowley, B. J. Thompson, M. J. Shearer, D. Ma, R. J. Hamers, J. C. Wright, S. Jin, *Journal of the American Chemical Society* **2015**, *137*, 5810.
[23]
[24] Z. Chen, Q. Dong, Y. Liu, C. Bao, Y. Fang, Y. Lin, S. Tang, Q. Wang, X. Xiao, Y. Bai, Y. Deng, J. Huang, *Nature communications* **2017**, *8*, 1890.
[25] A. a. O. El-Ballouli, O. M. Bakr, O. F. Mohammed, *Chemistry of Materials* **2019**.

[26] H. M. Zhu, Y. P. Fu, F. Meng, X. X. Wu, Z. Z. Gong, Q. Ding, M. V. Gustafsson, M. T. Trinh, S. Jin, X.-Y. Zhu, *Nature materials* **2015**, *14*, 636.
[27] Y. Fu, H. Zhu, C. C. Stoumpos, Q. Ding, J. Wang, M. G. Kanatzidis, X. Zhu, S. Jin, *ACS Nano* **2016**, *10*, 7963.
[28] Y. Cao, N. Wang, H. Tian, J. Guo, Y. Wei, H. Chen, Y. Miao, W. Zou, K. Pan, Y. He, H. Cao, Y. Ke, M. Xu, Y. Wang, M. Yang, K. Du, Z. Fu, D. Kong, D. Dai, Y. Jin, G. Li, H. Li, Q. Peng, J. Wang, W. Huang, *Nature* **2018**, *562*, 249.
[29] K. Lin, J. Xing, L. N. Quan, F. P. G. de Arquer, X. Gong, J. Lu, L. Xie, W. Zhao, D. Zhang, C. Yan, W. Li, X. Liu, Y. Lu, J. Kirman, E. H. Sargent, Q. Xiong, Z. Wei, *Nature* **2018**, *562*, 245.
[30] J. Luo, X. Wang, S. Li, J. Liu, Y. Guo, G. Niu, L. Yao, Y. Fu, L. Gao, Q. Dong, C. Zhao, M. Leng, F. Ma, W. Liang, L. Wang, S. Jin, J. Han, L. Zhang, J. Etheridge, J. Wang, Y. Yan, E. H. Sargent, J. Tang, *Nature* **2018**.
[31] L. T. Dou, Y. Yang, J. B. You, Z. R. Hong, W. H. Chang, G. Li, Y. Yang, *Nature communications* **2014**, *5*, 5404.
[32] W. Wei, Y. Zhang, Q. Xu, H. Wei, Y. Fang, Q. Wang, Y. Deng, T. Li, A. Gruverman, L. Cao, J. Huang, *Nat. Photon.* **2017**, *11*, 315.
[33] Q. Chen, J. Wu, X. Ou, B. Huang, J. Almutlaq, A. A. Zhumekenov, X. Guan, S. Han, L. Liang, Z. Yi, J. Li, X. Xie, Y. Wang, Y. Li, D. Fan, D. B. L. Teh, A. H. All, O. F. Mohammed, O. M. Bakr, T. Wu, M. Bettinelli, H. Yang, W. Huang, X. Liu, *Nature* **2018**, *561*, 88.
[34] Y. Zhang, R. Sun, X. Ou, K. Fu, Q. Chen, Y. Ding, L.-J. Xu, L. Liu, Y. Han, A. V. Malko, X. Liu, H. Yang, O. M. Bakr, H. Liu, O. F. Mohammed, *ACS Nano* **2019**, *13*, 2520.
[35] Y. F. Xu, M. Z. Yang, B. X. Chen, X. D. Wang, H. Y. Chen, D. B. Kuang, C. Y. Su, *Journal of the American Chemical Society* **2017**, *139*, 5660.
[36] M. Crespo-Quesada, L. M. Pazos-Outon, J. Warnan, M. F. Kuehnel, R. H. Friend, E. Reisner, *Nature communications* **2016**, *7*, 12555.
[37] J. Chen, J. Yin, X. Zheng, H. Ait Ahsaine, Y. Zhou, C. Dong, O. F. Mohammed, K. Takanabe, O. M. Bakr, *ACS Energy Lett.* **2019**.
[38] A. J. Bard, *J. Photochem.* **1979**, *10*, 59.
[39] A. Fujishima, K. Honda, *Nature* **1972**, *238*, 37.
[40] W.-Q. Wu, Z. Yang, P. N. Rudd, Y. Shao, X. Dai, H. Wei, J. Zhao, Y. Fang, Q. Wang, Y. Liu, Y. Deng, X. Xiao, Y. Feng, J. Huang, *Sci. Adv.* **2019**, *5*, eaav8925.
[41] S. Yang, Y. Wang, P. Liu, Y.-B. Cheng, H. J. Zhao, H. G. Yang, *Nat. Energy* **2016**, *1*, 15016.
[42] D. Ju, X. Zheng, J. Liu, Y. Chen, J. Zhang, B. Cao, H. Xiao, O. F. Mohammed, O. M. Bakr, X. Tao, *Angew. Chem. Int. Ed.* **2018**, *57*, 14868.
[43] X. Yang, L.-F. Ma, D. Yan, *Chem. Sci.* **2019**, *10*, 4567.
[44] Z.-J. Li, E. Hofman, J. Li, A. H. Davis, C.-H. Tung, L.-Z. Wu, W. Zheng, *Adv. Funct. Mater.* **2018**, *28*, 1704288.
[45] Z.-C. Kong, J.-F. Liao, Y.-J. Dong, Y.-F. Xu, H.-Y. Chen, D.-B. Kuang, C.-Y. Su, *ACS Energy Lett.* **2018**, *3*, 2656.
[46] Q. Zhong, M. Cao, H. Hu, D. Yang, M. Chen, P. Li, L. Wu, Q. Zhang, *ACS Nano* **2018**, *12*, 8579.
[47] A. Loiudice, S. Saris, E. Oveisi, D. T. L. Alexander, R. Buonsanti, *Angew. Chem. Int. Ed.* **2017**, *56*, 10696.
[48] A. Loiudice, M. Strach, S. Saris, D. Chernyshov, R. Buonsanti, *Journal of the American Chemical Society* **2019**, DOI: 10.1021/jacs.9b02061.
[49] S. Park, W. J. Chang, C. W. Lee, S. Park, H.-Y. Ahn, K. T. Nam, *Nat. Energy* **2016**, *2*, 16185.

[50] Y. Wu, P. Wang, X. Zhu, Q. Zhang, Z. Wang, Y. Liu, G. Zou, Y. Dai, M. H. Whangbo, B. Huang, *Adv. Mater.* **2018**, *30*, 1704342.
[51] Y. Wu, P. Wang, Z. Guan, J. Liu, Z. Wang, Z. Zheng, S. Jin, Y. Dai, M.-H. Whangbo, B. Huang, *ACS Catal.* **2018**, *8*, 10349.
[52] Z. Guan, Y. Wu, P. Wang, Q. Zhang, Z. Wang, Z. Zheng, Y. Liu, Y. Dai, M.-H. Whangbo, B. Huang, *Appl. Catal. B: Environ.* **2019**, *245*, 522.
[53] H. Wang, X. Wang, R. Chen, H. Zhang, X. Wang, J. Wang, J. Zhang, L. Mu, K. Wu, F. Fan, X. Zong, C. Li, *ACS Energy Lett.* **2018**, *4*, 40.
[54] L. Zhou, Y. F. Xu, B. X. Chen, D. B. Kuang, C. Y. Su, *Small* **2018**, *14*, e1703762.
[55] J. Hou, S. Cao, Y. Wu, Z. Gao, F. Liang, Y. Sun, Z. Lin, L. Sun, *Chem. Eur. J* **2017**, *23*, 9481.
[56] M. Ou, W. Tu, S. Yin, W. Xing, S. Wu, H. Wang, S. Wan, Q. Zhong, R. Xu, *Angew. Chem. Int. Ed.* **2018**, *57*, 13570.
[57] L.-Y. Wu, Y.-F. Mu, X.-X. Guo, W. Zhang, Z.-M. Zhang, M. Zhang, T.-B. Lu, *Angew. Chem. Int. Ed.* **2019**, 10.1002/anie.201904537.
[58] S. Wan, M. Ou, Q. Zhong, X. Wang, *Chem. Eng. J.* **2019**, *358*, 1287.
[59] P. Da, M. Cha, L. Sun, Y. Wu, Z. S. Wang, G. Zheng, *Nano letters* **2015**, *15*, 3452.
[60] H. Zhang, Z. Yang, W. Yu, H. Wang, W. Ma, X. Zong, C. Li, *Adv. Energy Mater.* **2018**, *8*, 1800795.
[61] I. Poli, U. Hintermair, M. Regue, S. Kumar, E. V. Sackville, J. Baker, T. M. Watson, S. Eslava, P. J. Cameron, *Nature communications* **2019**, *10*, 2097.
[62] C. Wang, S. Yang, X. Chen, T. Wen, H. G. Yang, *J. Mater. Chem. A* **2017**, *5*, 910.
[63] M. T. Hoang, N. D. Pham, J. H. Han, J. M. Gardner, I. Oh, *ACS applied materials & interfaces* **2016**, *8*, 11904.
[64] S. Nam, C. T. K. Mai, I. Oh, *ACS applied materials & interfaces* **2018**, *10*, 14659.
[65] R. Tao, Z. Sun, F. Li, W. Fang, L. Xu, *ACS Appl. Energy Mater.* **2019**, *2*, 1969.
[66] V. Andrei, R. L. Z. Hoye, M. Crespo-Quesada, M. Bajada, S. Ahmad, M. De Volder, R. Friend, E. Reisner, *Adv. Energy Mater.* **2018**, *8*, 1801403.
[67] L.-F. Gao, W.-J. Luo, Y.-F. Yao, Z.-G. Zou, *Chem. Commun.* **2018**, *54*, 11459.
[68] Y. S. Chen, J. S. Manser, P. V. Kamat, *Journal of the American Chemical Society* **2015**, *137*, 974.
[69] J. H. Kim, Y. Jo, J. H. Kim, J. W. Jang, H. J. Kang, Y. H. Lee, D. S. Kim, Y. Jun, J. S. Lee, *ACS Nano* **2015**, *9*, 11820.
[70] Gurudayal, D. Sabba, M. H. Kumar, L. H. Wong, J. Barber, M. Gratzel, N. Mathews, *Nano letters* **2015**, *15*, 3833.
[71] P. Dias, M. Schreier, S. D. Tilley, J. Luo, J. Azevedo, L. Andrade, D. Bi, A. Hagfeldt, A. Mendes, M. Grätzel, M. T. Mayer, *Adv. Energy Mater.* **2015**, *5*, 1501537.
[72] S. Xiao, C. Hu, H. Lin, X. Meng, Y. Bai, T. Zhang, Y. Yang, Y. Qu, K. Yan, J. Xu, Y. Qiu, S. Yang, *J. Mater. Chem. A* **2017**, *5*, 19091.
[73] J. Luo, Z. Li, S. Nishiwaki, M. Schreier, M. T. Mayer, P. Cendula, Y. H. Lee, K. Fu, A. Cao, M. K. Nazeeruddin, Y. E. Romanyuk, S. Buecheler, S. D. Tilley, L. H. Wong, A. N. Tiwari, M. Grätzel, *Adv. Energy Mater.* **2015**, *5*, 1501520.
[74] Y. Qiu, W. Liu, W. Chen, G. Zhou, P.-C. Hsu, R. Zhang, Z. Liang, S. Fan, Y. Zhang, Y. Cui, *Sci. Adv.* **2016**, *2*, e1501764.
[75] G. Segev, J. W. Beeman, J. B. Greenblatt, I. D. Sharp, *Nature materials* **2018**, *17*, 1115.
[76] Y. J. Jang, I. Jeong, J. Lee, M. J. Ko, J. S. Lee, *ACS Nano* **2016**, *10*, 6980.
[77] X. Zhang, B. Zhang, K. Cao, J. Brillet, J. Chen, M. Wang, Y. Shen, *J. Mater. Chem. A* **2015**, *3*, 21630.
[78] B. Sun, T. Shi, Z. Liu, Z. Tang, J. Zhou, G. Liao, *RSC Adv.* **2016**, *6*, 110120.
[79] J. H. Kim, Y. H. Jo, J. S. Lee, *Nanoscale* **2016**, *8*, 17623.

[80] Gurudayal, R. A. John, P. P. Boix, C. Yi, C. Shi, M. C. Scott, S. A. Veldhuis, A. M. Minor, S. M. Zakeeruddin, L. H. Wong, M. Gratzel, N. Mathews, *ChemSusChem* **2017**, *10*, 2449.
[81] J. H. Baek, B. J. Kim, G. S. Han, S. W. Hwang, D. R. Kim, I. S. Cho, H. S. Jung, *ACS applied materials & interfaces* **2017**, *9*, 1479.
[82] S. Wang, P. Chen, Y. Bai, J. H. Yun, G. Liu, L. Wang, *Adv. Mater.* **2018**, *30*, 1800486.
[83] X. Liu, Y. Wang, X. Cui, M. Zhang, B. Wang, M. Rager, Z. Shu, Y. Yang, Z. Li, Z. Lin, *J. Mater. Chem. A* **2019**, *7*, 165.
[84] J. Luo, D. A. Vermaas, D. Bi, A. Hagfeldt, W. A. Smith, M. Grätzel, *Adv. Energy Mater.* **2016**, *6*, 1600100.
[85] M. Schreier, L. Curvat, F. Giordano, L. Steier, A. Abate, S. M. Zakeeruddin, J. Luo, M. T. Mayer, M. Gratzel, *Nature communications* **2015**, *6*, 7326.
[86] G. Volonakis, F. Giustino, *Appl. Phys. Lett.* **2018**, *112*, 243901.

Jie Chen obtained his bachelor degree in Applied Chemistry from Xi'an Jiaotong University in 2011 and his PhD degree in Thermal Engineering under the supervision of Prof. Liejin Guo

from Xi'an Jiaotong University in 2017. During 2015-2017, he worked as a joint student in Department of Chemistry at UW-Madison under the supervision of Prof. Song Jin. He is currently a postdoctoral researcher working with Prof. Osman Bakr in the KAUST Catalysis Center. His research interests focus on functional nanomaterials for catalytic and optoelectronics applications.

((**For Essays, Feature Articles, Progress Reports, and Reviews,** please insert up to three author biographies and photographs here, max. 100 words each))

Author Photograph(s) ((40 mm broad, 50 mm high, gray scale))

The advancements made in the development of halide perovskites in photocatalyst particle-suspension systems, photoelectrode thin-film systems and photovoltaic-(photo)electrocatalysis systems for solar-chemical fuel conversion are reviewed. The syntheses and modification strategies established for yielding stable and efficient halide perovskites as well as the design of device configurations for water splitting, hydrogen iodide splitting, and CO_2 reduction are emphasized and discussed.

Keyword: solar fuel conversion, halide perovskite, CO_2 reduction, proton reduction

Jie Chen, Chunwei Dong, Omar F. Mohammed, Hicham Idriss, Osman M. Bakr*

Metal Halide Perovskites for Solar-to-Chemical Fuel Conversion